Fabrication of super-hydrophobic nickel film on copper substrate with improved corrosion inhibition by electrodeposition process

Zhen Yang [a,b], Xianping Liu [b], Yanling Tian [a,b,*]

[a]School of Mechanical Engineering, Tianjin University, Tianjin 300350, China

[b]School of Engineering, University of Warwick, Coventry CV4 7AL, UK

*Corresponding author e-mail address: meytian@tju.edu.cn

Abstract

Inspired by the famous "lotus effect", we have fabricated the super-hydrophobic surfaces with nickel film on copper substrates using a one-step electrodeposition method. By adjusting processing time, water contact angle of as-prepared surfaces can reach as high as 160.3 ± 1.5° with small rolling angle of 3.0 ± 0.5°, showing excellent super-hydrophobicity. After the deposition of nickel coating, the pristine copper surfaces became much rough with packed cauliflower-/thorn-like clusters. This unique surface texture contributed to trapping large amount of air and forming the air cushion underneath the water droplet, which can prevent the liquids contacting the copper substrate. The examination of surface chemical compositions implied that the deposited super-hydrophobic coating consisted of nickel crystals and nickel myristate. In this research, the formation mechanism of the electrodeposited super-hydrophobicity was extensively explained based on the analyses of surface texture and surface chemistry. Moreover, the corrosion resistance of the as-fabricated super-hydrophobic surface was estimated by the potentiodynamic polarization tests as well as the electrochemical impedance spectroscopy (EIS) measurements. The results demonstrate that the super-hydrophobic nickel coating showed excellent corrosion inhibition in simulated seawater solution. The existence of the super-hydrophobic coating could be regarded as a barrier and thus provide a perfect air-liquid interface that inhibits the penetration of the corrosive ions. This facile and effective method of electrodeposition process offers a promising approach for mass production of super-hydrophobic surfaces on various metals.

Keywords: Super-hydrophobic, Electrodeposition process, Corrosion resistance,

Copper, Nickel film

1. Introduction

Recently, super-hydrophobic surfaces have aroused tremendous interest in academic research and potential applications in industry owing to their great importance, such as self-cleaning capability [1], drag reduction [2], water/oil separation [3], corrosion resistance [4] and so on. Generally, super-hydrophobic surfaces present a water contact angle (WCA) over 150° with the lotus effect (rolling angle (RA) below 10°) or the pinning effect (no RA or RA above 10°) [5-6]. Studies on natural creatures with super-hydrophobic surfaces reveal that the presence of micro/nanostructured surface morphology is the main cause for constructing special surface wettability [7-9]. Besides, some special chemical components are also significant for the acquisition of super-hydrophobic surface [10-11]. Inspired by nature, two elements are preferable to obtain super-hydrophobicity: (1) a rough surface texture with unique binary structure and (2) modification of surface chemistry with low-free-energy coating [12].

So far, many different techniques have been proposed to successfully achieve bio-inspired super-hydrophobic surface through modifying surface morphology and surface chemical compositions including chemical vapor deposition [13]. sol-gel [14], chemical etching [15], laser surface texturing [8-10, 16], thermal embossing [17] and electrodeposition [18], etc. However, the first three mentioned techniques are limited due to expensive equipment, tedious chemical treatments and complicated multi-step processing procedures [19-20]. Regarding laser ablation method, although stable three-dimensional (3D) hierarchical structures can be acquired by its precise control, the previous studies proved that the fresh laser textured surfaces showed the hydrophilic or super-hydrophilic nature. It will take a relatively long time from serval days to several months under ambient air exposure to reach the super-hydrophobic state [21-23], which will limit the economic efficiency for any practical applications due to very long processing time. For thermal embossing approach, the micro/submicron periodic structures were imprinted on the thermoplastic polymers, but such surfaces cannot show super-hydrophobic property. In order to speed up the wettability transition process and quickly improve surface hydrophobicity, a post-processing was required to modify

surface chemistry using low-free-energy materials, such as per- and polyfluoroalkyl substances (PFASs) [24]. However, PFASs are considered as the global pollutants since they contain numerous manufactured nonbiodegradable compounds. In addition, an increasing body of evidence points to PFASs as environmental threat to kidney function [25-26]. Thus, the surface modification using PFASs is not an eco-friendly approach to produce super-hydrophobic surfaces. On the contrary, electrodeposition is a facile and one-step technique to create hierarchical surface texture and lower surface free energy at the same time. Beyond that, the surface wettability and surface morphology can be changed by altering processing parameters. It is therefore necessary to develop super-hydrophobic surfaces by means of electrodeposition process.

Copper is an important engineering material and it has a widespread industrial application, including heat conductors, electrical power lines and water supply pipelines [27]. However, the copper material will be easily corroded in wet environment, producing some toxic complexes, such as basic copper carbonate [$Cu_2(OH)_2CO_3$] and tribasic copper chloride [$Cu_2Cl(OH)_3$]. If copper material is used for water pipelines, these corrosion products can go into human stomach and then react with gastric acid to generate copper ion (Cu^{2+}). The continuous accumulation of heavy metal ion (Cu^{2+}) in body would cause the disruption of biochemical functions and cellular morphology by its toxicity [28]. Researchers proposed that the corrosion resistance will be remarkably enhanced through decreasing the contact area between the copper substrate and the corrosive liquids [29]. Therefore, it is urgent to develop super-hydrophobic coating produced on copper material to adjust its corrosion resistance. Nickel is an essential industrial material and it has good properties such as excellent corrosion resistance, high hardness and magnetism. If nickel is deposited on copper substrate, the deposited nickel will prevent the bare copper from corrosion [30]. With the combination of super-hydrophobicity, the deposited nickel film can present its unique advantages, which can broaden its applications including self-cleaning and corrosion resistance.

In this paper, the super-hydrophobic nickel film was rapidly constructed on the copper substrate using a single-step electrodeposition technique in ethanol electrolyte containing nickel chloride and myristic acid, which can avoid the post-processing of

surface treatment. The super-hydrophobic nickel film with the presence of cauliflower-/thorn-like rough structure and nonpolar functional groups contributed to excellent corrosion resistance for the bare copper substrate. This study is to reveal the influence of reaction time on surface morphology as well as wettability. Moreover, surface chemical compositions of the fabricated super-hydrophobic film were systematically examined by means of XPS and FT-IR. The results indicate that the deposited coating was composed of nickel crystals and nickel myristate, which can dramatically lower surface free energy. Both the surface morphology and chemical compositions were carefully analyzed to reveal the formation mechanism of the electrodeposited super-hydrophobic film. This method of electrodeposition process is very simple, low-cost and effective, which offers a promising approach for mass production of super-hydrophobic surface on various metals.

2. Experimental

2.1. Materials and chemicals

Copper (purity 99%) substrate with the size of 30 × 10 × 1 mm^3 was investigated in this study. Anhydrous ethanol, acetone, sodium chloride, myristic acid, nickel chloride and other alkalis were used as received (analytical grade). A commercial UCP-III water purification system was employed to provide distilled water.

2.2. Sample preparation

Nickel films were electrodeposited on copper using direct current (DC). Prior to electrodeposition process, abrasive SiC papers (2000 grit) were utilized to mechanically polish the copper substrates. Then the polished samples were washed by an ultrasonic bath containing acetone, ethanol and distilled water in sequence each for 5 min to remove surface contaminations. In order to degrease the polished copper substrates, they were ultrasonically cleaned using home-made alkaline solution having 20 g/L NaOH, 10 g/L Na_2CO_3, 25 g/L NaH_2PO_4 and 25 g/L Na_2SiO_3 for 5 min at 60ºC. Subsequently, the samples were activated in 10 wt.% HCl for 30s, flushed by distilled water, and then, immediately placed in the electroplating bath. Nickel chloride ($NiCl_2 \cdot 6H_2O$, 19 g/L) as ions source and myristic acid ($CH_3(CH_2)_{12}COOH$, 22.8 g/L) as surface chemical modifier were poured into anhydrous ethanol under constant

stirring until 150 ml uniform electrolytic solution was prepared. Two copper substrates with the distance of 2 cm were taken as anode and cathode in the electrodeposition system, and a DC voltage of 30 V was performed to the two copper electrodes. The electrolysis time was set at 1, 5, 10 and 20 min, the working cathodic surface was rinsed with distilled water and then dried in air, achieving the super-hydrophobic copper surface with nickel film. For reference, another electrodeposited sample was produced on copper substrate in ethanol electrolyte with nickel chloride but in absence of myristic acid for 10 min, which was abridged as electrodeposited Ni. Besides, a flat nickel plate was immersed into anhydrous ethanol containing myristic acid (22.8 g/L) for 10 min at room temperature.

2.3. Measurement and characterization

Surface morphology of the super-hydrophobic surfaces was detected by scanning electron microscopy (SEM, model: FEI Quanta 250). A contact angle meter (model: AST VCA optima) was employed to measure WCA and RA using 8 μL distilled water droplet at room condition of temperature 25ºC and humidity 50%. The WCA and RA values were recorded immediately after electrodeposition and no obvious changes of contact angles were observed in the following two weeks. Average values with standard deviation were reported in this study. Fourier transform infrared spectroscopy (FT-IR, model: Thermo Scientific, Nicolet iS50) and X-ray photoelectron spectroscopy (XPS, model: Thermo Scientific, Escalab 250Xi) were applied to examine the surface chemical compositions.

A standard three-electrode configuration was performed to evaluate the electrochemical corrosion resistance, the bare copper substrate, electrodeposited Ni and the super-hydrophobic surface that was deposited for 10 min as the working electrode (exposed area of 1 cm^2), a platinum plate as counter electrode (CE) and the saturated calomel electrode (SCE) as the reference electrode (RE). Corrosion tests were conducted in the simulated seawater of 3.5 wt.% aqueous NaCl solution to acquire the potentiodynamic polarization curves and electrochemical impedance spectroscopy (EIS) using an electrochemical workstation (CHI660D, China) at room temperature. Prior to electrochemical measurements, the substrates were placed in corrosive solution for 30

min to allow the system stabilized. A sweep rate of 10 mV/s was set to receive the potentiodynamic polarization plots. The Tafel linear extrapolation method from polarization plot was utilized to calculate the corrosion parameters. The frequency range was fixed between 10^5 to 10^{-2} Hz with a sinusoidal amplitude of 10 mV in the electrochemical impedance microscopy (EIS) experiments.

3. Results and discussion

3.1. Surface morphology and wettability

Surface morphology of the as-fabricated cathodic surface with different reaction time is studied in this research. Fig. 1 displays SEM images of the fabricated nickel films under reaction time for (a, b) 1, (c, d) 5, (e, f) 10, and (g, h) 20 min, respectively. It is observed that the micro-sized clusters with nano-sized particles (as shown the yellow circles in Fig. 1) were packed on the copper substrates, resulting in a tidy and uniform surface with lots of protrusions. For 1 min electrodeposition time, the nickel ions (Ni^{2+}) around the cathodic electrode would quickly receive electrons, and numerous pure nickel nucleus (Ni) were deposited on the cathodic copper electrode with the applied DC voltage. At the same time, some nickel ions could react with myristic acid producing nickel myristate. The continuously formed fresh nickel nucleus can contribute to the growth of nickel myristate. As clearly shown in the magnified SEM image of Fig. 1(b), the as-prepared surface showed a rough cauliflower-like morphology due to the presence of formed nickel and nickel myristate particles [31]. It reveals that the cauliflower-like particles had a diameter of 200-400 nm, and the micro-sized clusters were formed when several cauliflower-like particles combined together. As the electroplating time was prolonged to 5-20 minuntes, it is obvious that the fabricated surfaces presented the thorn-like surface structure and the rough surfaces were covered by particles with an increased diameter of more than 500 nm. Besides, there were many cracks covered on these particles, resulting in much trapped air among the cracks. The air cushion could noticeably decrease the contact area between the sample surface and the liquids, thus the suspended liquid droplets hardly penetrate into the fabricated surface, showing a super-hydrophobic property. However, the diameter of the particles enlarged and the electrodeposited film became thick due to the extension

of electroplating time, as shown in Fig. 1(d, f). As a result, the nickel film became even more densely and there was less trapped air among the particles at the 20 min electrodeposition time, as displayed in Fig. 1(h).

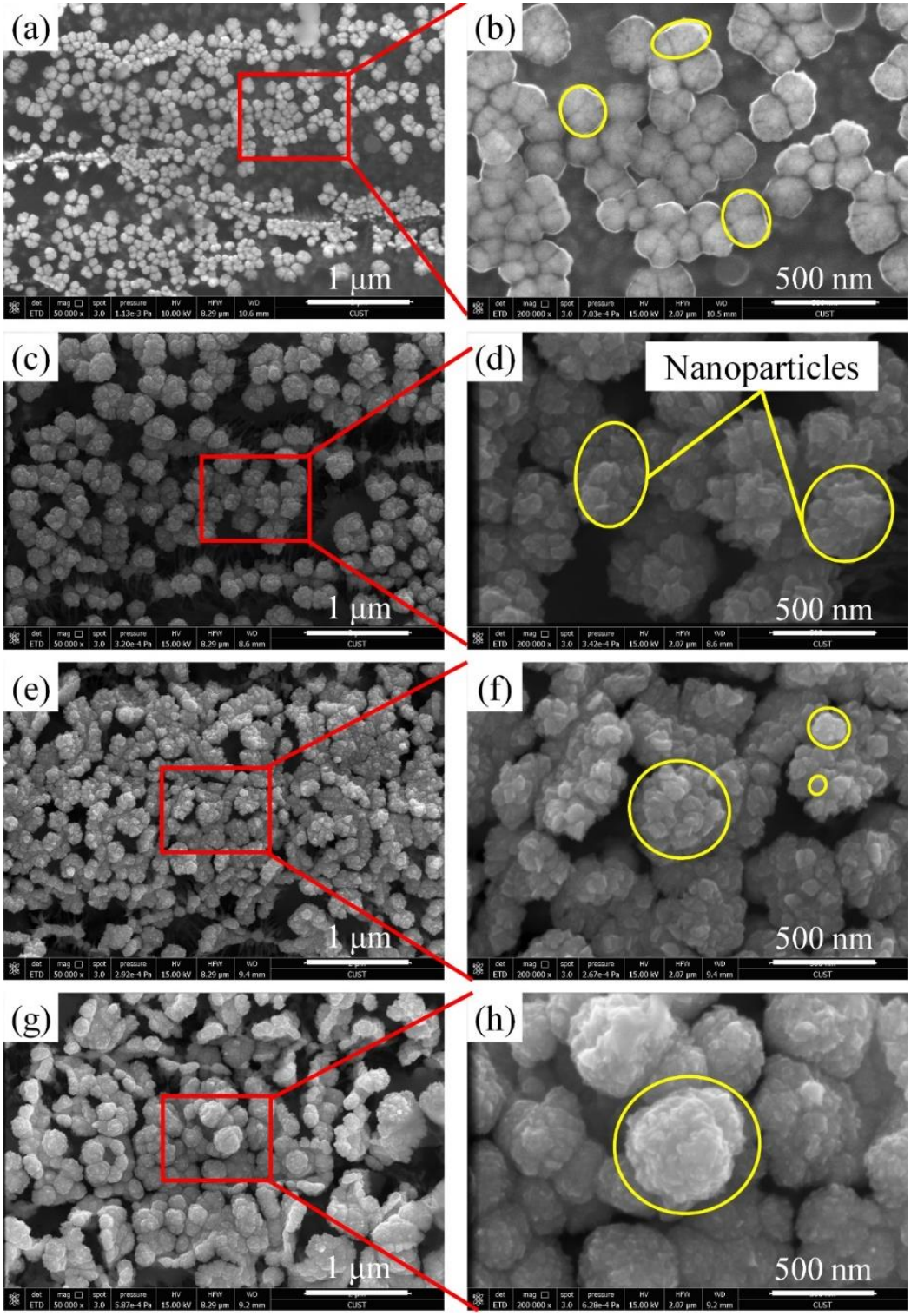

Figure 1. SEM images of nickel film versus electrolysis time with different magnification, (a, b) 1 min (c, d) 5 min, (e, f) 10 min, (g, h) 20 min.

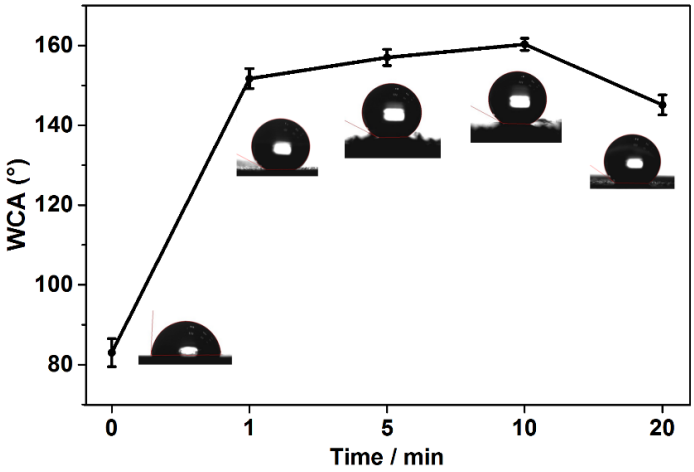

Figure 2. Variation for WCA of the deposited surfaces under different processing time.

The influence of various reaction time on surface wettability is explored in this study. The samples were fabricated under 0, 1, 5, 10 and 20 min processing time at 30 V voltage in the ethanol solution with nickel chloride and myristic acid. The difference of WCAs under various processing time is shown in Fig. 2. The WCA of the copper substrate is 83.0 ± 3.5° with no existence of RA, showing a typical hydrophilic nature. It can be noted that when electrolysis time was extended to 1 min, the super-hydrophobic film could be acquired with the WCA of 151.8 ± 1.5° and RA of 6.0 ± 1.5°. The results reveal that the WCAs presented an increase trend with the extension of reaction time in 10 min, and the WCA could reach as high as 160.3 ± 1.5° with a smaller RA of 3.0 ± 0.5°. But the WCA would decrease as the reaction time was further prolonged to 20 min, indicating that long processing time resulted in too dense micro/nano structures and too thick deposited nickel film on the copper substrate. This may reduce the proportion of trapped air among the formed particles, and thus weaken the super-hydrophobic property.

3.2. Surface chemistry

XPS and FTIR were employed to analyze the surface chemical compositions of the sample. As shown in Fig. 3, XPS spectra can further present more details of the surface chemistry. Obviously, three peak signals of C 1s, O 1s and Ni 2p were presented in the XPS survey spectrum of the fabricated super-hydrophobic coating. According to their corresponding atomic concentration, the atomic ratio of C/O/Ni can be approximately calculated to 28:4:1, which is in agreement with the nickel myristate

stoichiometry ($Ni[CH_3(CH_2)_{12}COO]_2$). Noticeably, the as-prepared surface had the highest carbon content of 84.05% compared with oxygen and nickel. We conjecture that the formed nickel myristate contributed to the increase of surface carbon content, and the super-hydrophobicity was ascribed to the introduced nonpolar functional groups of C-C(H) from nickel myristate. This conclusion coincides with previous studies: the increase of carbon content results in enhancement of surface hydrophobicity owing to the presence of low-free-energy functional groups of $-CH_2$ and $-CH_3$ [20, 32].

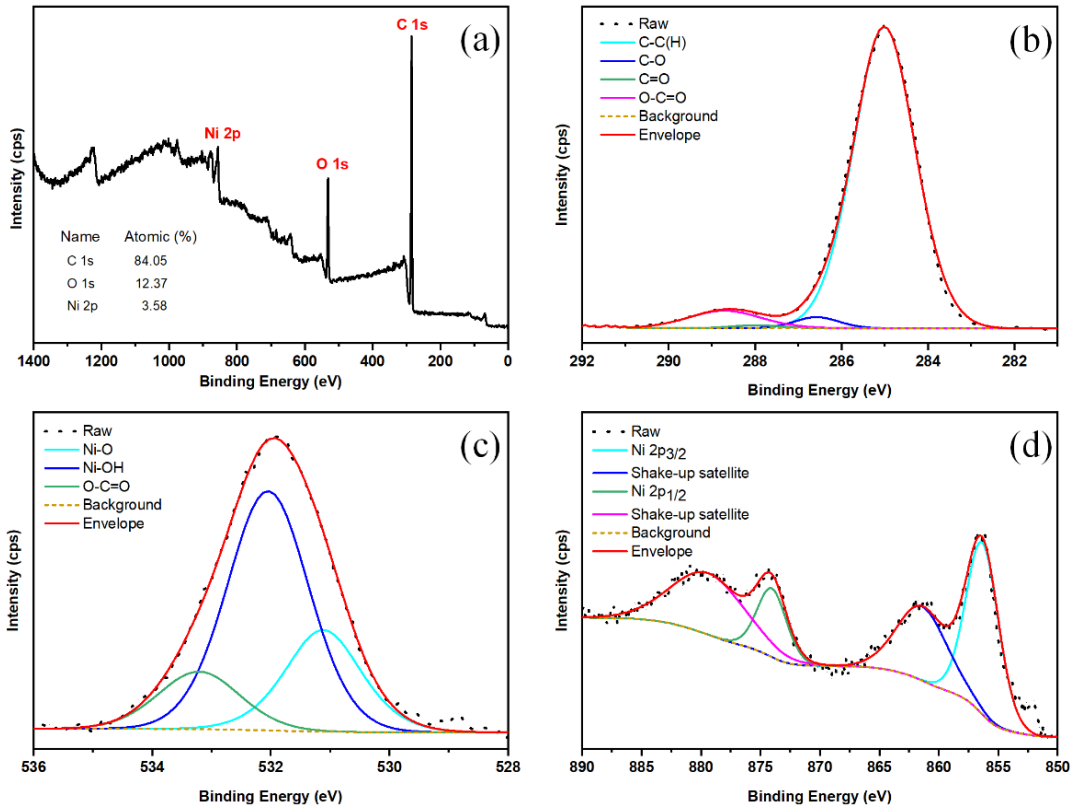

Figure 3. XPS spectra of the super-hydrophobic surface: (a) survey spectrum, (b) C 1s region, (c) O 1s region, (d) Ni 2p region.

Besides, the decompositions of C 1s, O 1s and Ni 2p peaks were conducted to insight into the inherent feature of the deposited film. Fig. 3(b) displays the high resolution of C 1s spectrum, and two strong peaks locating at 285.0 and 288.8 eV were related to C-C(H) and O=C-O moieties, respectively, further demonstrating that the long chain molecules of myristic acid were attached on the as-prepared nickel film. The other two weak peaks at 286.5 and 287.4 eV corresponded to C-O and C=O moieties, respectively. The polar moieties of C-O and C=O might derive from the corresponding residual liquid after cleaning procedure using ethanol and acetone. Beyond that, the

chemisorbed organic matters from air and the residual oil in the XPS vacuum chamber are other sources to increase the amount of the four abovementioned functional groups [21-22, 33-34]. However, the result implied that the as-prepared surface was dominated by the nonpolar C-C(H) groups with the concentration of 90.62% as shown in the Fig. 3(b). Therefore, the total amount of other three polar functional groups had little effect on the surface wettability due to very low content, resulting in a relatively stable super-hydrophobicity on the as-fabricated surface.

Fig. 3(c) depicts the high resolution of O 1s spectrum. The fitted peak locating at 531.1 eV was assigned to the Ni-O species and another binding energy at about 533.2 eV was related to the O-C=O groups. The obvious peak at 532.0 eV corresponded to the Ni-OH species. The reason is that the pure nickel was deposited on the copper substrate during the electroplating process, then the fresh nickel crystal would hydroxylated when reacted with the hydroxyl ions. We conjecture that two main sources of hydroxyl ions contributed to the hydroxylation effect. The first one is the crystal water from nickel chloride ($NiCl_2 \cdot 6H_2O$) due to the electrolytic dissociation effect. Another one is the residual distilled water. This is because, after electrodeposition process, the as-prepared surfaces were rinsed with distilled water and dried in the ambient air. As a result, the freshly formed nickel crystal would be hydroxylated in the wet environment. The high resolution of Ni 2p spectrum is exhibited in Fig. 3(d). It is noted that there are two peaks locating at 856.3 and 874.2 eV, which were contributed to Ni 2p3/2 and Ni 2p1/2, respectively [35]. Beyond, other two weak peaks at 861.3 and 879.5 eV were assigned to shake-up satellites of Ni 2p, implying that the valence state of the Ni atom on the super-hydrophobic nickel film is Ni^{2+} [36]. Thus the XPS results prove that nickel myristate ($Ni[CH_3(CH_2)_{12}COO]_2$) with low-free-energy functional groups was successfully deposited on the copper substrate.

FT-IR was employed to further explore the functional groups on the as-prepared super-hydrophobic nickel coating. As shown in Fig. 4, in high-frequency region, the absorption peak at 2954 cm^{-1} was related to the asymmetric vibration of $-CH_3$ [37]. The bands at around 2920 and 2850 cm^{-1} were ascribed to the asymmetric and symmetric stretching vibrations of C-H group [31]. The peaks at 1409 and 1545 cm^{-1} in low-

frequency region stem from symmetric and asymmetric stretches of coordinated O-C=O moieties [38]. Thus, it can be concluded that the obtained film should be nickel complex with organic acid. All above analyses confirm that the low-surface-energy compounds were deposited on the copper substrate, which contributed to the super-hydrophobic performance.

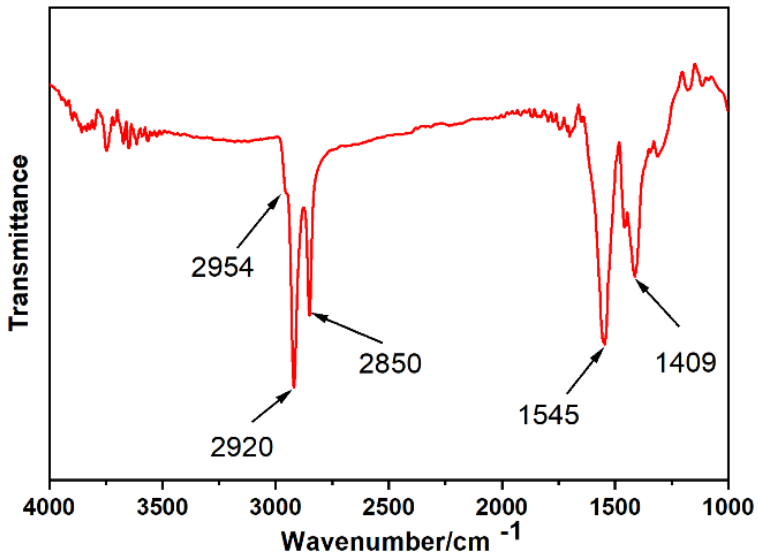

Figure 4. FT-IR spectrum of the fabricated super-hydrophobic nickel film.

3.3.Formation mechanism

The surface chemistry analyses reveal that the as-prepared super-hydrophobic coating with protrusive clusters was comprised of nickel (Ni) and nickel myristate ($Ni[CH_3(CH_2)_{12}COO]_2$). The possible formation mechanism is illustrated in Fig. 5. Nickel ions (Ni^{2+}) would move to the cathodic electrode and quickly get electron to generate pure nickel (Ni) under the applied DC voltage between the two copper electrodes. Besides, there were many nickel ions (Ni^{2+}) around the cathodic copper electrode reacting with myristic acid to generate the nickel myristate. The freshly formed nickel nucleus contributed to the anisotropy crystal growth of nickel myristate [39]. Therefore, the appearance of nickel myristate ($Ni[CH_3(CH_2)_{12}COO]_2$) resulted from the reaction of nickel ions and myristic acid under the application of DC voltage, which led to the presence of low-surface-energy functional groups ($-CH_3$ and $-CH_2$) on the as-prepared super-hydrophobic surface. Meanwhile, some hydrogen ions (H^+) around the cathodic plate also gained electrons to produce the hydrogen (H_2) during the electroplating process. The released gas led to the loose morphology on the obtained

super-hydrophobic surface. Once the liquid droplet was placed on the such surface, many air pockets would be trapped underneath the droplet owing this unique surface structure, resulting in super-hydrophobic performance. The whole reactions processes on cathodic electrode can be explained by the following formulas:

$$Ni^{2+} + 2e^{-} \rightarrow Ni \quad (1)$$

$$Ni^{2+} + 2CH_3(CH_2)_{12}COOH \rightarrow Ni[CH_3(CH_2)_{12}COO]_2 + 2H^{+} \quad (2)$$

$$2H^{+} + 2e^{-} \rightarrow H_2(g) \quad (3)$$

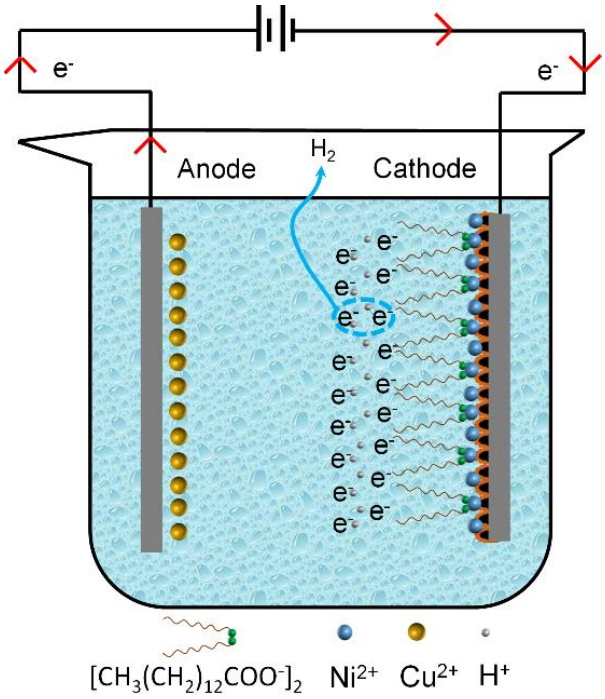

Figure 5. Schematic diagram of the electrodeposition process for the fabrication of super-hydrophobic nickel film.

Two essential features are generally required to produce super-hydrophobic surface: a nonpolar surface chemistry combined with a micro/nanostructured surface texture. Apart from the analyses of surface chemical compositions, based on Cassie-Baxter equation, the influence of surface structure on the fabrication mechanism of super-hydrophobic surface is also discussed below [40].

$$\cos\theta_{CB} = f_1 \cos\theta_0 - f_2 \quad (4)$$

where f_1 denotes the fractional area of solid surface that is wetted by water droplet and f_2 presents the proportion of air in contact with water droplet; θ_{CB} (160.3º) denotes the WCA of the electrodeposited super-hydrophobic surface with 10 min processing time.

θ_0 is more suitable to present the WCA of a flat nickel surface modified with myristic acid for 10 min, and its WCA of 95.6º is recorded. Given that $f_1 + f_2 = 1$, f_1 can be calculated at 0.065, which reveals that 93.5% of the contact area was between water droplet and trapped air. Since air shows absolute hydrophobicity, the unique surface structures with large amount of trapped air is therefore responsible for the super-hydrophobicity. It is concluded that the fabricated cathodic copper substrates with micro/nanostructured surface and the introduced low-surface-energy functional groups showed excellent super-hydrophobicity.

3.4. Corrosion resistance

In order to explore corrosion resistance, the potentiodynamic polarization tests and EIS measurements were employed to examine the bare copper substrate, electrodeposited Ni and the super-hydrophobic coating in simulated seawater solution containing 3.5 wt.% NaCl. Fig. 6(a) shows the schematic diagram of the experimental setup and the potentiodynamic polarization plots are displayed in the Fig. 6(b).

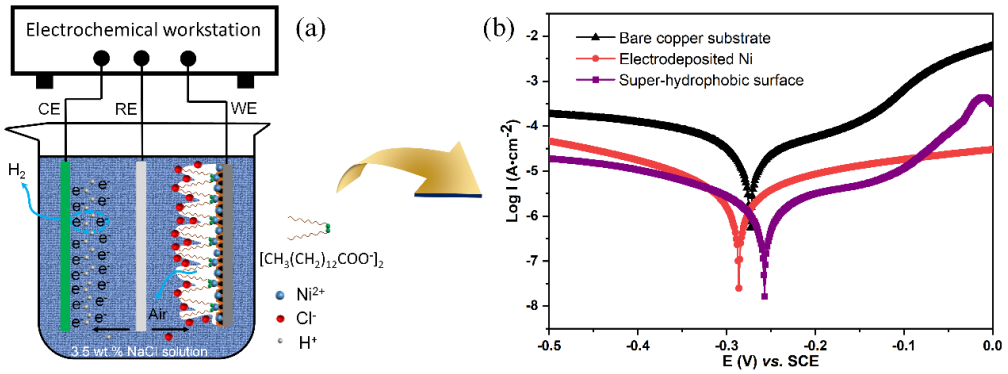

Figure 6. (a) Schematic diagram of the potentiodynamic polarization tests: WE: working electrode, CE: counter electrode, RE: reference electrode; (b) potentiodynamic polarization curves for bare copper substrate, electrodeposited Ni and the super-hydrophobic surface.

The corrosion current density (I_{corr}) and corrosion potential (E_{corr}) can be achieved by extrapolating the linear portions of the potentiodynamic polarization plots to the intersection. Meanwhile, the corrosion rate (CR, mm/a) can be calculated according to the following equation [41]:

$$CR = \frac{K \times I_{corr} \times M}{D \times V} \quad (5)$$

where K is constant at 3270. M, D and V are molecular weight, valence and mass density of copper, respectively. Their corresponding corrosion potential, corrosion current

density and corrosion rate are summarized in Table 1. The lower corrosion current density and corrosion rate imply that the electrodeposited Ni had better corrosion resistant performance than the pristine copper substrate. As expected, the super-hydrophobic nickel film presented the best corrosion resistance compared with the electrodeposited Ni and the bare copper substrate. The corrosion rate of the as-fabricate super-hydrophobic surface decreased a staggering 16-fold from the bare copper substrate, which demonstrated that the corrosion resistance of bare copper substrate was significantly enhanced owing to the presence of the electrodeposited super-hydrophobic nickel coating.

Table 1. Corrosion potential (E_{corr}), corrosion current density (I_{corr}) and corrosion rate (CR) of the bare copper substrate, electrodeposited Ni and the super-hydrophobic surface.

Sample	E_{corr} (V)	I_{corr} (A cm^{-2})	CR (mm a^{-1})
Bare copper substrate	-0.27	4.8×10^{-5}	5.6×10^{-1}
Electrodeposited Ni	-0.28	9.7×10^{-6}	1.0×10^{-1}
Super-hydrophobic surface	-0.25	3.0×10^{-6}	3.5×10^{-2}

Corrosion resistance of the electrodeposited super-hydrophobic surface was further evaluated using the powerful electrochemical impedance spectroscopy (EIS). Fig. 7 shows their corresponding Nyquist plots and Bode plots. As known, the diameter of Nyquist loop refers to the polarization resistance of the working electrode in corrosion process. Obviously, the electrodeposited super-hydrophobic surface presented the largest loop due to the protective coating of nickel and myristic acid, followed by electrodeposited Ni coating. The bare copper substrate had the smallest Nyquist loop, indicating that it would be easily corroded in the NaCl solution compared to the electrodeposited Ni and the super-hydrophobic surface. Fig. 7(b) shows the Bode plots (log impedance modulus |Z| versus log frequency) of the three surfaces. Noticeably, the bare copper substrate possessed the lowest impedance modulus |Z| in low frequency range, while the as-fabricated super-hydrophobic surface had the largest impedance modulus |Z|. These results can confirm that deposited super-hydrophobic coating can perform excellent corrosion resistance to protect the bare copper material.

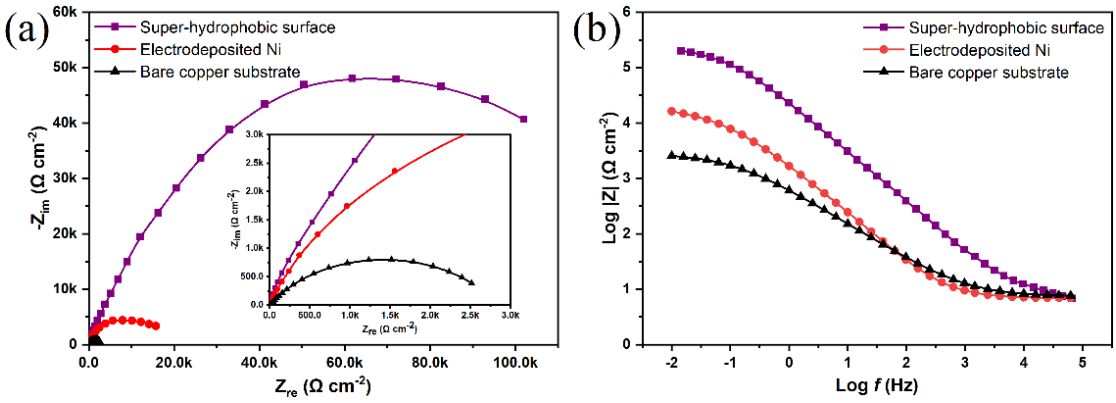

Figure 7. (a) Nyquist plots and (b) Bode plots of the bare copper substrate, electrodeposited Ni and the super-hydrophobic nickel coating in 3.5 wt.% aqueous NaCl solution.

In order to further analyze the impedance data of these three samples, various equivalent circuits were applied to fit the Nyquist plots (as shown in Fig. 8). All the capacitors were substituted by the mathematically modelled constant phase element (CPE) because the actual electrochemical corrosion process is not the pure capacitor. The CPE impedance can be expressed by the following mathematical equation:

$$Z_{CPE} = Y_0^{-1}(\mathrm{j}w)^{-n} \tag{6}$$

where $\mathrm{j}^2 = -1$, w (rad/s) denotes the angular frequency, Y_0 (μSs^{n}cm^{-2}) represents the CPE constant. n is the CPE exponent with a range between 0 and 1 [37, 42].

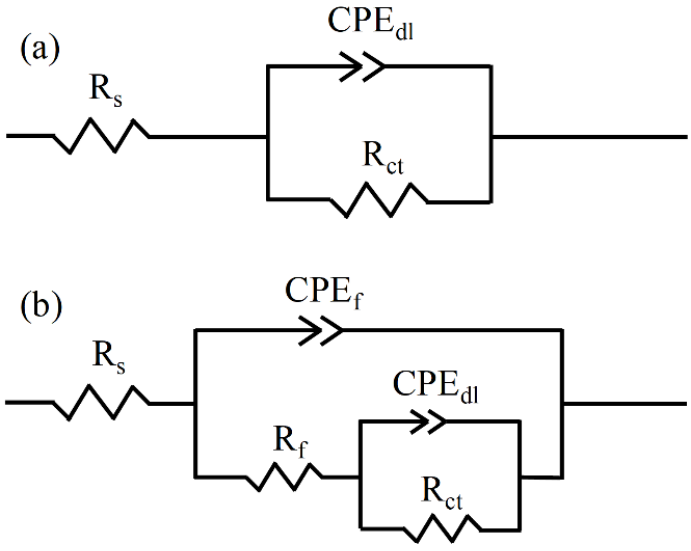

Figure 8. Equivalent circuit diagram of the studied system: (a) for bare copper substrate, (b) for electrodeposited Ni as well as the as-prepared super-hydrophobic surface.

Fig. 8(a) shows the equivalent circuit modelling of the bare copper substrate, where the electrolyte resistance is denoted by R_s, charge transfer resistance is described by R_{ct}, and the CPE_{dl} represents the constant phase element of the electrical double

layer [30]. The performance of surface corrosion resistance can be characterized by the value of R_{ct}. Both the electrodeposited Ni and the prepared super-hydrophobic surface can be modelled by the same equivalent circuit as shown in Fig. 8(b). In this circuit, R_s is the resistance of electrolytic solution, R_f and CPE_f represent the resistance and the constant phase element of the deposited Ni film or the super-hydrophobic coating. $R_{ct}||CPE_{dl}$ components mean the impedance with the interface reaction between the electrodeposited film and the copper substrate [20]. Better fitting results can be achieved using the equivalent circuit model presented in Fig. 8(b) for Ni film as well as the as-fabricated super-hydrophobic surface. In Table 2, the simulated data of circuit elements are presented. By comparing the R_{ct} values, the bare copper substrate had the lowest value of 2.82 $k\Omega cm^2$, gradual increase to 9.73 $k\Omega cm^2$ for the electrodeposited Ni sample, and the super-hydrophobic surface presented the largest value of 140.26 $k\Omega cm^2$. As clearly seen in Table 3 and Fig. 8, the results reveal that the electrodeposited nickel film with myristic acid play a significant role in improving corrosion resistance for the pristine copper substrate.

Table 2. Parameters extracted from Nyquist plots using equivalent circuit modelling.

Sample	R_{ct}	CPE_{dl}		R_f	CPE_f		R_s
	($k\Omega cm^2$)	Y_0	n	($k\Omega cm^2$)	Y_0	n	(Ωcm^2)
Bare copper	2.82	43.35	0.66	-	-	-	5.24
Electrodeposited Ni	9.73	16.22	0.57	8.69	11.36	0.87	7.09
Super-hydrophobic	140.26	13.88	0.54	73.47	1.03	0.91	7.38

As schematically illustrated by Fig. 6(a), the protrusive clusters with covered cracks as well as the presence of absorbed low-free-energy functional groups on the electrodeposited coating contributed to its excellent corrosion resistance. This unique surface morphology can contribute to forming many air pockets, and the corrosive medium (Cl^-) will be suspended on the interface. Besides, the attached nonpolar functional groups of $-CH_3$ and $-CH_2$ also repel the liquid droplets to penetrate into the surface. The harmful ions cannot easily contact the bare copper substrates due to the generation of air cushion in this case. Thus, the electrodeposited super-hydrophobic coating can effectively protect the copper substrate from corrosion.

4. Conclusions

In summary, a deposited super-hydrophobic nickel coating on copper substrate was successfully prepared by the one-step electrodeposition technique, and its improvement of corrosion resistance was also studied. The processing time was optimized and the static WCA can be as high as 160.3 ± 1.5° with a small RA of 3.0 ± 0.5°. The SEM images indicate that the copper surface became much rough with packed micro/nanoscale cauliflower-/thorn-like clusters after the deposition of nickel film. Such unique surface texture can contribute to trapping large amount of air, and the air cushion would prevent the water droplet from penetrating into the copper surface, showing a super-hydrophobic property. The results of surface chemical compositions confirm that the super-hydrophobic surfaces were comprised of nickel crystals (Ni) and nickel myristate crystals ($Ni[CH_3(CH_2)_{12}COO]_2$). FT-IR spectrum further confirm that the nonpolar functional groups of ($-CH_3$ and $-CH_2$) were attached on the copper substrate, which can lower the surface free energy and contribute to super-hydrophobicity. The formation mechanism of the electrodeposited super-hydrophobic coating was schematically illustrated. Compared with the pristine copper, the fabricated super-hydrophobic surface behaved better corrosion resistance, which can be proved by the potentiodynamic polarization tests and EIS measurements. It is therefore assumed that the corrosion performance was consistent with surface wettability, because the super-hydrophobic surface can prevent the corrosive ions (Cl^-) to contact the bare metal surface. The electrodeposition process is very simple and fast, which offers an effective approach to produce super-hydrophobic surface with improved corrosion inhibitive property on a variety of metals.

Acknowledgements

This work received financial supports from Program of International S&T Cooperation (2016YFE0112100), H2020-MSCA-RISE Project (FabSurfWAR-644971), National Key R&D Program of China (No. 2017YFB1104700) and National Natural Science Foundations of China (Nos. 51675371, 51675376 and 51675367). We also acknowledge the technique supports from Prof. Zuobin Wang and Prof. Zhankun Weng in Changchun University of Science and Technology.

References:

[1] L.J. Xiao, W.G. Zeng, G.F. Liao, C.F. Yi, Z.S. Xu, Thermally and chemically stable candle soot superhydrophobic surface with excellent self-cleaning properties in air and oil, ACS Appl. Nano Mater. 1 (2018) 1204-1211.

[2] N. Wang, L.L. Tang, Y.F. Cai, W. Tong, D.S. Xiong, Scalable superhydrophobic coating with controllable wettability and investigations of its drag reduction, Colloids Surf., A, 555 (2018) 290-295.

[3] Y.W. Cai, S. Li, Z.L. Cheng, G.Y. Xu, X.J. Quan, Y.T. Zhou, Facile fabrication of super-hydrophobic FAS modified electroless Ni-P coating meshes for rapid water-oil separation, Colloids Surf., A, 540 (2018) 224-232.

[4] Y.B. Zhao, L.Q. Shi, X.J. Ji, J.C. Li, Z.Z. Han, S.L. Li, R.C. Zeng, F. Zhang, A.L. Wang, Corrosion resistance and antibacterial properties of polysiloxane modified layer-by-layer assembled self-healing coating on magnesium alloy, J. Colloid. Interface. Sci. 526 (2018) 43-50.

[5] C.V. Ngo, D.M. Chun, Control of laser-ablated aluminum surface wettability to superhydrophobic or superhydrophilic through simple heat treatment or water boiling post-processing, Appl. Surf. Sci. 435(2018) 974-982.

[6] M. Psarski, J. Marczak, J. Grobelny, G. Celichowski, Superhydrophobic surface by replication of laser micromachined pattern in epoxy/alumina nanoparticle composite, J. Nanomater. 2 (2014) 105-119.

[7] J.L. Yong, Q. Yang, F. Chen, D.S. Zhang, U. Farooq, G.Q. Du, X. Hou, A simple way to achieve superhydrophobicity, controllable water adhesion, anisotropic sliding, and anisotropic wetting based on femtosecond laser-induced line-patterned surfaces, J. Mater. Chem. A 2 (2014) 5499-5507.

[8] Z. Yang, Y.L. Tian, C.J. Yang, F.J. Wang, X.P. Liu, Modification of wetting property of Inconel 718 surface by nanosecond laser texturing, Appl. Surf. Sci. 414 (2017) 313-324.

[9] C.J. Yang, X.S. Mei, Y.L. Tian, D.W. Zhang, Y. Li, X.P. Liu, Modification of wettability property of titanium by laser texturing, Int. J. Adv. Manuf. Technol. 87 (2016) 1663-1670.

[10] Y.L. Tian, Y.C. Zhao, C.J. Yang, F.J. Wang, X.P. Liu, X.B. Jing, Fabrication of bio-inspired nitinol alloy surface with tunable anisotropic wetting and high adhesive ability, J. Colloid. Interface. Sci. 527 (2018) 328-338.

[11] H. Li, S. Yu, X. Han, Y. Zhao, A stable hierarchical superhydrophobic coating on pipeline steel surface with self-cleaning, anticorrosion, and anti-scaling properties, Colloids Surf., A, 503 (2016) 43-52.

[12] F.H. Su, K. Yao, Facile fabrication of superhydrophobic surface with excellent mechanical abrasion and corrosion resistance on copper substrate by a novel method, ACS Appl. Mater. Interfaces 6 (2014) 8762-8770.

[13] S.A. Kamal, R. Ritikos, S.A. Rahman, Wetting behavior of carbon nitride nanostructures grown by plasma enhanced chemical vapor deposition technique, Appl. Surf. Sci. 328 (2015) 146-153.

[14] R.V. Lakshmi, B.J. Basu,Fabrication of superhydrophobic sol-gel composite films using hydrophobically modified colloidal zinc hydroxide, J. Colloid. Interface. Sci. 339 (2009) 454-460.

[15] J. Cremaldi, B. Bhushan, Fabrication of bioinspired, self-cleaning superliquiphilic/phobic stainless steel using different pathways, J. Colloid. Interface. Sci. 518 (2018) 284-297.

[16] M.M. Calderon, A. Rodriguez, A.D. Ponte, M.C. Morant-Minana, M.G. Aranzadi, S.M. Olaizola, Femtosecond laser fabrication of highly hydrophobic stainless steel surface with hierarchical structures fabricated by combining ordered microstructures and LIPSS, Appl. Surf. Sci. 374 (2016) 81-89.

[17] S.F. Toosi, S. Moradi, M. Ebrahimi, S.G. Hatzikiriakos, Microfabrication of polymeric surfaces with extreme wettability using hot embossing, Appl. Surf. Sci. 378 (2016) 426-434.

[18] Y. Huang, D.K. Sarkar, D. Gallant, X.G. Chen, Corrosion resistance properties of superhydrophobic copper surfaces fabricated by one-step electrochemical modification process, Appl. Surf. Sci. 282 (2013) 689-694.

[19] Z.X. She, Q. Li, Z.W. Wang, L.Q. Li, F.N. Chen, J.C. Zhou, Novel method for controllable fabrication of a super-hydrophobic CuO surface on AZ91D

magnesium alloy, ACS Appl. Mater. Interfaces 4 (2012) 4348-4356.

[20] Y. Liu, S.Y. Li, J.J. Zhang, J.A. liu, Z.W. Han, L.Q. Ren, Corrosion inhibition of biomimetic super-hydrophobic electrodeposition coatings on copper substrate, Corros. Sci. 94 (2015) 190-196.

[21] J. Long, M. Zhong, H. Zhang, P. Fan, Superhydrophilicity to superhydrophobicity transition of picosecond laser microstructured aluminum in ambient air, J. Colloid Interf. Sci. 441 (2015) 1-9.

[22] Z. Yang, X.P. Liu, Y.L. Tian, Insights into the wettability transition of nanosecond laser ablated surface under ambient air exposure, J. Colloid Interface Sci. 533 (2019) 268-277.

[23] D.V. Ta, A. Dunn, T.J. Wasley, R.W. Kay, J. Stringer, P.J. Smith, C. Connaughton, J.D. Shephard, Nanosecond laser textured superhydrophobic metallic surfaces and their chemical sensing applications, Appl. Surf. Sci.357 (2015) 248-254.

[24] B.X. Zheng, G.D. Jiang, W.J. Wang, X.S. Mei, Fabrication of superhydrophilic or superhydrophobic self-cleaning metal surfaces using picosecond laser pulses and chemical fluorination, Radiat. Eff. Defects Solids 171 (2016) 461-473.

[25] J.W. Stanifer, H.M. Stapleton, T. Souma, A. Wittmer, X.L. Zhao, L.E. Boulware, Perfluorinated chemicals as emerging environmental threats to kidney health, Clin J. Am. Soc. Nephrol. (2018) https://doi.org/10.2215/CJN.04670418.

[26] J. Ju, X. Yao, X. Hou, Q.H. Liu, Y.S. Zhang, A. Khademhosseini, A highly stretchable and robust non-fluorinated super-hydrophobic surface, J. Mater. Chem. A 5 (2017) 16273-16280.

[27] Y.H. Fan, Z.J. Chen, J. Liang, Y. Wang, H. Chen, Preparation of superhydrophobic films on copper substrate for corrosion protection, Surf. Coat. Technol. 244 (2014) 1-8.

[28] S.N. Padrilah, M.K. Sabullah, M.Y.A. Shukor, N.A. Yasid, N.A. Shamaan, S.A. Ahmad, Toxicity effects of fish histopathology on copper accumulation, Pertanika J. Trop. Agric. Sci. 41 (2018) 519-540.

[29] P. Wang, D. Zhang, R. Qiu, Liquid/solid contact mode of super-hydrophobic film in aqueous solution and its effect on corrosion resistance, Corros. Sci. 54 (2012)

77-84.

[30] S. Khorsand, K. Raeissi, F. Ashrafizadeh, Corrosion resistance and long-term durability of super-hydrophobic nickel film prepared by electrodeposition process, Appl. Surf. Sci. 305 (2014) 498-505.

[31] Z. Chen, L.M. Hao, A.Q. Chen, Q.J. Song, C.L. Chen, A rapid one-step process for fabrication of super-hydrophobic surface by electrodeposition method, Electrochim. Acta, 59 (2012) 168-171.

[32] H. Bagheri, M. Aliofkhazraei, H.M. Forooshani, A.S. Rouhaghdam, Facile fabrication of uniform hierarchical structured (UHS) nanocomposite surface with high water repellency and self-cleaning properties, Appl. Surf. Sci. 436 (2018) 1134-1146.

[33] J.T. Cardoso, A. Garcia-Girón, J.M. Romano, D. Huerta-Murillo, R. Jagdheesh, M. Walker, S.S. Dimov, J.L. Ocaña, Influence of ambient conditions on the evolution of wettability properties of an IR-, ns-laser textured aluminium alloy, RSC Adv. 7 (2017) 39617-39627.

[34] J. Long, M. Zhong, P. Fan, D. Gong, H. Zhang, Wettability conversion of ultrafast laser structured copper surface, J. Laser Appl. 27 (2015) S29107.

[35] X. Chen, Y. He, Y. Fan, Q.B. Yang, G.Y. Zeng, H, Shi, Facile fabrication of a robust superwetting three-dimensional (3D) nickel foam for oil/water separation, J. Mater. Sci. 52 (2017) 2169-2179.

[36] T. Yoshida, K. Yamasaki K, The core-level binding energies and the structures of nickel complexes, Bull. Chem. Soc. Jpn. 54 (1981) 935-936.

[37] Y. Liu, X.M. Yin, J.J. Zhang, S.Y. Yu, Z.W. Han, L.Q. Ren, A electro-deposition process for fabrication of biomimetic super-hydrophobic surface and its corrosion resistance on magnesium alloy, Electrochim. Acta, 125 (2014) 395-403.

[38] Z. Chen, L.M. Hao, C.L. Chen, A fast electrodeposition method for fabrication of lanthanum super-hydrophobic surface with hierarchical micro-nanostructures, Colloids Surf. A 401 (2012) 1-7.

[39] Y.C. Zhu, H.G. Zheng, Q. Yang, A.L. Pan, Z.P. Yang, Y.T. Qian, Growth of dendritic cobalt nanocrystals at room temperature, J. Cryst. Growth 260 (2004)

427-434.

[40] A.B.D. Cassie, S. Baxter, Wettability of porous surfaces, Trans. Faraday Soc. 40 (1944) 546-551.

[41] D. Prasai, J. Tuberquia, R. Harl, G. Jennings, K. Bolotin, Graphene: corrosion-inhibiting coating, ACS Nano 6 (2012) 1102-1108.

[42] Z.Q. Yang, L.D. Wang, W. Sun, S.J. Li, T.Z. Zhu, W. Liu, G.C. Liu, Superhydrophobic epoxy coating modified by fluorographene used for anti-corrosion and self-cleaning, Appl. Surf. Sci. 401 (2017) 146-155.